J Biol Inorg Chem (2011) 16:157–172
DOI 10.1007/s00775-010-0714-2

ORIGINAL PAPER

Characterization of structure and activity of garlic peroxidase (POX_{1B})

Sarra El Ichi · Anna Miodek · Hélène Sauriat-Dorizon · Jean-Pierre Mahy · Céline Henry · Mohamed Nejib Marzouki · Hafsa Korri-Youssoufi

Received: 18 March 2010 / Accepted: 4 October 2010 / Published online: 2 November 2010

Abstract Structural characterization and study of the activity of new POX_{1B} protein from garlic which has a high peroxidase activity and can be used as a biosensor for the detection of hydrogen peroxide and phenolic compounds were performed and compared with the findings for other heme peroxidases. The structure–function relationship was investigated by analysis of the spectroscopic properties and correlated to the structure determined by a new generation of high-performance hybrid mass spectrometers. The reactivity of the enzyme was analyzed by studies of the redox activity toward various ligands and the reactivity with various substrates. We demonstrated that, in the case of garlic peroxidase, the heme group is pentacoordinated, and has an histidine as a proximal ligand. POX_{1B} exhibited a high affinity for hydrogen peroxide as well as various reducing cosubstrates. In addition, high enzyme specificity was demonstrated. The k_{cat} and K_M values were 411 and 400 mM^{-1} s^{-1} for 3,3′,5,5′-tetramethylbenzidine and 2′-azinobis(3-ethylbenzothiazoline-6-sulfonic acid), respectively. Furthermore, the reduction of nitro compounds in the presence of POX_{1B} was demonstrated by iron(II) nitrosoalkane complex assay. In addition, POX_{1B} showed a great potential for application for drug metabolism since its ability to react with 1-nitrohexane in the presence of sodium dithionite was demonstrated by the appearance of a characteristic Soret band at 411 nm. The high catalytic efficiency obtained in the case of the new garlic peroxidase (POX_{1B}) is suitable for the monitoring of different analytes and biocatalysis.

Keywords Peroxidase · Heme protein · Catalytic activity · Ligand · Nitrosoalkane

S. El Ichi · A. Miodek · H. Sauriat-Dorizon · J.-P. Mahy · H. Korri-Youssoufi (✉)
Equipe de Chimie Bioorganique et Bioinorganique,
Institut de Chimie Moléculaire et Matériaux d'Orsay,
UMR8182, CNRS,
Université Paris-Sud,
91405 Orsay, France
e-mail: hafsa.korri-youssoufi@u-psud.fr

S. El Ichi · M. N. Marzouki
Bioengineering Unit 99 UR 09-26,
National Institute of Applied Sciences and Technology,
7th November University at Carthage,
Centre Urbain Nord, BP 676-1080,
Tunis Cedex, Tunisia

C. Henry
Unité BioBac, INRA UR477,
Jouy-en-Josas, France

Introduction

Peroxidases are oxidoreductases found in plants, microorganisms, and animals [1, 2]. These enzymes have many applications in enzyme immunoassays [3], medical diagnostics [4, 5], detoxification of wastewater, industrial waste treatment [6], and biosensors for the determination of glucose, alcohols, glutamate and choline [7], hydrogen peroxide [8, 9], and phenolic compounds [10]. These applications arise from the high activity of peroxidases in the presence of a wide range of organic and inorganic compounds that can be oxidized in the presence of hydrogen peroxide. Substrate discrimination is controlled, in the active site, by the protein backbone, which protects the heme active species during turnover [11]. In fact, structural studies of plant peroxidases have revealed that they are heme proteins containing iron(III) protoporphyrin IX (ferriprotoporphyrin IX) as the prosthetic group (except the glutathione peroxidase, which has a selenocysteine

residue at the active site). The first 3D structure of a peroxidase to be determined was that of yeast cytochrome *c* peroxidase [12]. Later, 3D structures were obtained for several peroxidases, including lignin peroxidase [13], pea cytosolic ascorbate peroxidase [14], peanut peroxidase (PNP) [15], and horseradish peroxidase (HRP) [16]. All of them are proteins with 300–400 amino acids and their molecular masses range from 30,000 to 150,000 Da. In general, within a particular class 35–95% sequence homology can be observed, whereas between different classes the sequence homology is less than 20% [17]. In fact, the heme complex consists of a protoporphyrin ring, which contains a central iron(III) ion, which is bound to the four pyrrolic nitrogens in the equatorial plane and to two axial ligands; one being provided by the apoprotein on the proximal face of the heme and the other, on the distal face of the heme, being exogenous [18, 19]. Consequently, some structural differences due to the orientation of the axial ligands could be pointed out by analyzing the paramagnetic shifts of the heme methyl groups in NMR spectroscopy [20]. The heme is the key component for hemoproteins involved in oxidative metabolism, electron transfer processes [21], and biological systems [22, 23]. Heme is a good reservoir to pool electrons or positive holes, and thus provides the redox potential required for a variety of catalytic reactions (oxidation, peroxidation, oxygenation, and peroxygenation). Many of the enzymes containing heme utilize this property to activate relatively stable oxygen species such as hydrogen peroxide (H_2O_2) and molecular oxygen (O_2). The oxidative capacity of heme peroxidases is determined by a combination of factors, such as active-site topology, substrate accessibility, and redox potential [24, 25]. The properties of peroxidases can also be affected by several other factors, such as the number and nature of the axial ligands, the spin and oxidation state of the iron, and the proximal and distal residues [26]. In heme proteins, the presence of generally only one strong axial ligand on the proximal face of the heme allows access of other reactive species to the sixth coordination site of the iron on the distal face of the heme [27]. The redox properties and the accessibility of the iron are affected by the chemical nature of the axial ligand(s) [28, 29]. In fact, the chemical catalysis has been reported to be related to the nature of the axial ligand. The differences in the protein structural features near the heme binding site and the axial ligation to the heme iron lead to the functional differentiation of heme proteins having the same prosthetic group such as hemoglobin, myoglobin, cytochromes, and peroxidases [30]. Peroxidases contain either a cysteine-coordinated iron (chloroperoxidase) or a histidine-coordinated iron (thyroid peroxidase, myeloperoxidase…). In the case of PNP and HRP, His169 is the fifth ligand of the heme iron. His169 is hydrogen-bonded to the carboxylate group of Asp239 [31]. The nature of the fifth ligand can affect the electronic structure and reactivities of heme proteins [32–34]. HRP has two histidine residues which have different roles depending on their position: the distal histidine acts as a general base and is involved in the deprotonation/protonation of substrates during the catalytic cycle, whereas the heme iron is strongly coordinated by the proximal histidine [35, 36]. The relationship between the position of the distal histidine and the peroxidase activity has been demonstrated by studies on HRP C mutants [37]. The geometry of the histidine axial ligand, the presence of hydrogen bonds involving its imidazole moiety, the presence of a sixth ligand, and other heme deformations might influence the spin state [38].

In addition to their ability to oxidize a wide range of cosubstrates, the formation of iron(II) nitrosoalkane complexes extends the versatility of peroxidases [39]. These enzymes, like HRP [40] and other heme proteins such as cytochrome P-450 [41], hemoglobin, myoglobin [42], and prostaglandin synthase [43], catalyze the oxidation of alkylhydroxylamines or other primary amines, producing stable iron(II) nitrosoalkane complexes. Nitrosoalkanes belong to the family of C-nitroso compounds having a nitroso group which is isoelectronic with dioxygen. These compounds are known to form heme–nitrosoalkane bonds [44]. Such compounds can be generated not only by the reduction of nitro compounds but also by the oxidative metabolism of drugs containing reactive amines. In some heme proteins, stabilization of the nitrosoalkane ligand occurs via a hydrogen bond between the nitroso oxygen atom and the distal pocket histidine residue, such as His64 in myoglobin [44, 45]. The formation of protein–iron(II) nitrosoalkane complexes (metabolic intermediate complexes) is particularly important since they have an inhibitory effect and can be formed by oxidation of amine functions of drugs, thus causing severe toxic side effects [46, 47].

A novel peroxidase from garlic named POX_{1B} has been purified recently [48]. This enzyme shows a high peroxidase activity which is reasonably stable with temperature and time, and which makes it highly interesting for several applications such as in biosensors devices [49, 50]. The present work presents the structure and activity studies which have been performed to understand the structure–function relationships in garlic peroxidase POX_{1B}. Spectroscopic investigations of POX_{1B} were first carried out, to characterize the coordination chemistry of the heme iron. The nature of the axial ligand in the native protein was determined by matrix-assisted laser desorption/ionization (MALDI) time-of-flight (TOF) mass spectrometry (MS) and POX_{1B} was validated by nano high-performance liquid chromatography (HPLC) coupled with tandem MS (LC–MS/MS). The redox activity and the effect of the axial

ligands of the heme were analyzed by cyclic voltammetry, and the kinetic parameters of the peroxidase reaction were also determined for the oxidation of different cosubstrates in the presence of hydrogen peroxide as an oxidant. Finally, the ability of POX_{1B} to form iron(II) nitrosoalkane complexes upon reduction of nitro compounds was demonstrated.

Materials and methods

Materials

Ferriprotoporphyrin IX chloride, hydrogen peroxide, 2,2′-azinobis(3-ethylbenzothiazoline-6-sulfonic acid) (ABTS), 3,3′,5,5′-tetramethylbenzidine (TMB), *o*-dianisidine, guaiacol, pyridine, imidazole, nitrohexane, and nitrocyclohexane, were purchased from Sigma-Aldrich. 2-Butanone (99%) and sodium dithionite were purchased from Acros Organics and Merck, respectively. All reagents were of the highest purity and all the solutions were prepared with deionized water.

Purification of native and reconstituted POX_{1B}

Native protein POX_{1B} was purified from garlic bulb (*Allium sativum* L.) by ammonium sulfate precipitation, gel filtration, and anion-exchange chromatography [48]. After anion-exchange chromatography, the active fractions of the native POX_{1B} were lyophilized and stored at 4 °C for further experiments.

Reconstitution of POX_{1B}

Ferriprotoporphyrin IX chloride (1 mg/5 mL 1.4 M NH_4OH) was used for the reconstitution of POX_{1B}. The apoprotein was first obtained by extraction of the heme remaining in purified POX_{1B} by 2-butanone at 0 °C. For this, a solution of purified native POX_{1B} in 25 mM tris(hydroxymethyl)aminomethane (Tris)–HCl buffer pH 7.5 was treated by an equal volume of 2-butanone at 0 °C. The resulting protein solution was then analyzed by UV–vis spectroscopy to check that no native heme was remaining as proven by the lack of absorbance at 405 nm. To reconstitute POX_{1B}, the apoprotein was then incubated with a solution of commercial hemin chloride (1 mg mL^{-1} in dimethyl sulfoxide) for 15 min at room temperature (20 °C). Free heme was then separated from the reconstituted hemoprotein by gel chromatography (14 cm × 1.5 cm, Sephadex G-25, Sigma-Aldrich). Fractions of 1 mL were eluted using 25 mM Tris–HCl buffer pH 7.5 as the eluent. The protein content of each fraction was determined by the Bradford method [51] using bovine serum albumin as a standard. Their peroxidase activity was assayed by monitoring the increase of the absorbance at 460 nm for the oxidation of 0.79 mM *o*-dianisidine by 10 mM H_2O_2 in 100 mM sodium acetate buffer pH 5 in the presence of a 15-μL aliquot of each fraction [52]. The heme content was quantified by measurement of the absorbance at 405 nm. The fractions which contained heme but displayed no peroxidase activity were discarded. The active fractions were lyophilized and the resulting reconstituted POX_{1B} was stored at 4 °C for further experiments.

Electrophoresis

Sodium dodecyl sulfate polyacrylamide gel electrophoresis (SDS-PAGE) was performed in a vertical gel apparatus (Mini-Protean, Bio-Rad) with 10% polyacrylamide gel, as described by Laemmli [53]. Samples containing approximately 10 μL taken from a 1 mg mL^{-1} protein solution were applied to the gel and electrophoresed at 90 V for 1 h. Proteins were stained using a modified sensitive procedure as described by Hoopes and Dean [54]. The gel was incubated in a solution containing 50 mM sodium acetate (pH 5.0), 1% dimethyl sulfoxide, and 2 mM 1,8-diaminonaphthalene. Hydrogen peroxide was added at a final concentration of 5 mM. The gel was incubated at 20 °C for about 5 min. The gel was immersed in 20% trichloroacetic acid before staining with 0.2% (w/v) Coomassie brilliant blue in 50% (v/v) methanol and 7.5% (v/v) acetic acid for 60 min and destaining was performed with a solution containing 50% (v/v) methanol and 10% (v/v) acetic acid. Molecular weight markers (SDS 7, Sigma-Aldrich) were used.

Spectroscopic studies

Absolute and differential UV–vis absorption spectra were recorded with a UVIKON 860 UV–vis spectrophotometer. For the differential spectra, a solution of POX_{1B} (0.6 μM in 10 mM phosphate buffer pH 7.4) was prepared from the lyophilized powder. It was then equally divided into two 1-mL cuvettes, one being used as the reference cuvette and the other one, where reactants were added, being used as a sample cuvette. Spectroscopic studies were first performed using native POX_{1B} protein. Then, reconstituted POX_{1B} was used to study enzyme kinetics, coordination of axial ligands on the heme iron, and formation of iron(II) nitrosoalkane complexes. Measurements without the apoprotein were performed under the same conditions, using solutions of commercial hemin as controls to validate the spectroscopic results. Suitable volumes of sodium dithionite, pyridine, and imidazole were taken from 10 mM stock solutions in 0.1 mM phosphate buffer pH 7.4. Measurements were made in duplicate, at room temperature (20 °C)

under anaerobic conditions. All buffers were degassed by nitrogen bubbling.

Validation of POX_{1B}-heme by LC–MS/MS

In the current study, the identity of peptides was obtained by a MALDI–TOF MS system (Voyager DE super STR, Applied Biosystems, Foster City, USA) equipped with a nitrogen laser emitting at 337 nm. The peptide (1.2 mg) was resuspended in 100 μL of 0.3% trifluoroacetic acid (TFA). One microliter of peptide was mixed on the stainless steel MALDI plate with 1 μL of α-cyano-4-hydroxycinnamic acid (Sigma-Aldrich, Saint-Quentin-Fallavier, France) and 10 mM ammonium phosphate (Sigma-Aldrich, Saint-Quentin-Fallavier, France) at 4 mg mL^{-1} in acetonitrile (ACN)/0.3% TFA (50:50; v/v) and dried at room temperature. Spectra were recorded in positive reflector mode with an accelerating voltage of 20 kV, a delayed extraction time of 130 ns, and a 62% grid voltage. Spectra were calibrated using an external calibrator—Des Arg-1 bradykinin $(M+H)^+ = 904.46$ (Sequazyme peptide mass standards kit, Applied Biosystems, Foster City, USA)—and mass spectra were treated by Data Explorer 4.2 (Applied Biosystems) with the following parameters: noise filter/smooth (noise removal of 1). Spectral profiles were collected in the mass range $m/z = 400$–1,200.

Determination of the proximal ligand by MS

The LC–MS/MS (U 3000 Dionex, LTQ Orbitrap, Thermo Electron) analysis was performed using slices extracted from the Coomassie- and silver-stained SDS-PAGE gels. Proteins were reduced and alkylated before direct in-gel tryptic digestion. Proteins were identified by a mass-matching approach. HPLC was performed with an Ultimate 3000 LC system (Dionex). A 4-μL sample was loaded at 20 μL min^{-1} on a precolumn cartridge (stationary phase C_{18} PepMap 100, 5 μm; column 300-μm inner diameter, 5 mm; Dionex) and desalted with 0.08% TFA and 2% ACN. After 4 min, the precolumn cartridge was connected to the separating PepMap C_{18} column (stationary phase C_{18} PepMap 100, 3 μm; column 75-μm inner diameter, 150 mm; Dionex). The buffers were 0.1% HCOOH and 2% ACN (buffer A) and 0.1% HCOOH and 80% ACN (buffer B). The peptide separation was achieved with a linear gradient from 0 to 36% buffer B for 18 min at 300 nL min^{-1}. Including the regeneration step at 100% buffer B and the equilibration step at 100% buffer A, one run took 50 min. Eluted peptides were analyzed online with an LTQ Orbitrap mass spectrometer (Thermo Electron) using a nanoelectrospray interface. Ionization (1.3-kV ionization potential) was performed with a liquid junction and a capillary probe (10-μm inner diameter; New Objective). Peptide ions were analyzed using Xcalibur 2.07 with the following data-dependent acquisition steps (1): full MS scan in the orbitrap (m/z 300–1,600, profile mode) and (2) MS/MS in the linear trap ($qz = 0.25$, activation time 30 ms, and collision energy 45%; centroid mode). The second step was repeated for the four major ions detected in the first step. The dynamic exclusion time was set to 90 s.

Raw data obtained from the LC–MS/MS spectra were analyzed by BioWorks 3.3.1 SP1 (Sequest). A database search was performed with BioWorks 3.3.1 (Thermo Electron). We looked for trypsin digestion, cysteine carboxyamidomethylation (static), and methionine oxidation (possible modifications). The precursor mass and fragment mass tolerance were 1 Da and 10 ppm, respectively. The Viridiplantae protein database (641,746 entries, 18 July 2007 update) and the sequence of HRP (Swiss-Prot entry P00433) were used. The tryptic peptides identified were filtered according to the cross-correlation score, greater than 1.7, 2.2, and 3.3 for peptides with one, two, and three charges, respectively, and each with a probability below 0.05. At least two different peptides were required.

Electrochemical studies

The protein sample (50 μL of a 2 μM solution of POX_{1B} in 25 mM Tris–HCl buffer pH 7.5) was introduced into an electrochemical cell equipped with a gold disk as the working electrode, a platinum mesh as the counter electrode, and Ag/AgCl as the reference electrode. An Autolab PGSTA 100 potentiostat controlled by Autolab software (GPES) was used for the electrochemical measurements. Cyclic voltammetry measurements were achieved at a scan rate of 50 mV s^{-1} using a sweep potential from −0.3 to +0.6 V.

Catalytic activity of POX_{1B}

The peroxidase activity was assayed in the presence of different reducing cosubstrates—ABTS, TMB, *o*-dianisidine, and guaiacol—using hydrogen peroxide as an oxidant. The absorbance was monitored in the presence of ABTS, TMB, *o*-dianisidine, and guaiacol, respectively, at 414 nm ($\varepsilon = 28{,}000\ M^{-1}\ cm^{-1}$), 650 nm ($\varepsilon = 13{,}600\ M^{-1}\ cm^{-1}$), 460 nm ($\varepsilon = 11{,}300\ M^{-1}\ cm^{-1}$), and 470 nm ($\varepsilon = 3{,}800\ M^{-1}\ cm^{-1}$) using a UVIKON 860 UV–vis spectrometer. Various concentrations between 0.01 and 0.1 mM for ABTS and TMB, and between 0.1 and 1 mM for *o*-dianisidine and guaiacol were used in the presence of 10 mM H_2O_2 as an oxidant considered as a saturated concentration. The preliminary determination of the rate of the reaction of POX_{1B} with H_2O_2 was carried out by measuring the absorbance of the Soret band of the heme at 406 nm ($\varepsilon = 105{,}000\ M^{-1}\ cm^{-1}$) as a function of time in

the presence of increasing concentrations of H_2O_2 (1–11 mM). All measurements were done at optimal pH and ionic strength (0.1 M sodium acetate buffer pH 5) and at 25 °C using 2 μM POX_{1B} in 10 mM phosphate-buffered saline (PBS) pH 7.4. The measurements were repeated six times to test the reproducibility. k_{cat} and K_M values were determined from Lineweaver–Burk plots.

Reactions of POX_{1B} with nitroalkanes

Differential spectra were recorded as described in "Spectroscopic studies." Increasing concentrations of sodium dithionite (0.12–0.36 mM) were added to the enzyme solution (0.6 μM in 10 mM PBS pH 7.4). The heme reduction was confirmed by the appearance of a peak at 411 nm characteristic of high-spin hexacoordinated species. The nitro compound (1-nitrohexane) was added at concentrations from 0.1 to 0.8 mM and the absorbance was monitored between 350 and 750 nm. All measurements were made at room temperature (20 °C) under anaerobic conditions.

Results and discussion

Native protein POX_{1B} was purified from garlic bulbs (*A. sativum* L.) by ammonium sulfate precipitation, followed by gel filtration and anion-exchange chromatography [48]. POX_{1B} was biochemically characterized and it was shown to be highly active at acidic pH and stable with regard to temperature and storage either in solution in 25 mM Tris–HCl pH 7.5 or immobilized in biopolymers [48, 49]. Overall, as will be shown later, the catalytic activity and properties of this enzyme appeared to be similar to those of HRP, which also contains iron(III) protoporphyrin IX as a prosthetic group. The first part of the structure–function relationship studies consisted in the determination of the molecular mass of POX_{1B}. The protein migrated at approximately 30 kDa in the SDS-PAGE gel as well as under nondenaturating conditions in the presence of molecular weight markers. The protein band was revealed by Coomassie blue staining in the first case and by an activity assay in the presence of *o*-dianisidine in the second case (data not shown). According to these findings, the molecular mass of native POX_{1B} was evaluated to be 30 kDa, which is within the molecular mass range (28–60 kDa) of plant isoperoxidases [55]. It is noteworthy that POX_{1B} has a smaller molecular mass than HRP, the molecular mass of which is in the 40–45-kDa range [56].

Structural studies of native POX_{1B}

The UV–vis absorption spectrum of native POX_{1B} (Fig. 1, spectrum a) was typical of a high-spin hexacoordinate species, like in many other heme peroxidases. Indeed, the electronic absorption spectrum of POX_{1B} shows a Soret band at 406 nm ($\varepsilon = 105{,}000\ M^{-1}\ cm^{-1}$), which is similar to spectra reported for other plant peroxidases such as HRP and tobacco peroxidase (Soret band for both enzymes at 403 nm, $\varepsilon = 102{,}000\ M^{-1}\ cm^{-1}$) [57, 58] and lignin and manganese peroxidases (Soret band for both enzymes at 409 nm, $\varepsilon = 165{,}000\ M^{-1}\ cm^{-1}$) [59]. Protein purity ($A_{280}$) and heme content ($A_{406}$) were assessed by the A_{406}/A_{280} ratio corresponding to the Reinheitszah (RZ) value. The RZ value was 0.36, suggesting that the POX_{1B} protein did not contain 100% heme (i.e., the heme-to-apoprotein ratio was less than 1). To confirm the presence of iron(III) protoporphyrin IX as the prosthetic group, heme extraction was performed in the presence of 2-butanone at 0 °C. The UV–vis analysis of the butanone extract showed a Soret band at 396 nm that was typical of iron(III) protoporphyrin IX under those conditions, demonstrating that iron(III) protoporphyrin IX is the prosthetic group of garlic peroxidase.

Pyridine was used as a standard external ligand of the heme iron in coordination chemistry studies. When pyridine (2 mM) was added to the solution of enzyme (0.6 μM in 10 mM PBS pH 7.4) in its oxidized iron(III) state, the Soret peak shifted to 420 nm (Fig. 1, spectrum b). After reduction in the presence of sodium dithionite, and in presence of pyridine as an external ligand, a new spectrum with a Soret peak at 422 nm and two additional absorption bands at 530 and 560 nm were observed (Fig. 1, spectrum c). The spectrum obtained was similar to the spectra obtained for other heme proteins such as cyclooxygenase [60] and microperoxidase 8 [61] when reduced by sodium dithionite in the presence of a large excess of pyridine. It could thus be assigned either to a POX_{1B}Fe(II)(His)(pyridine) complex,

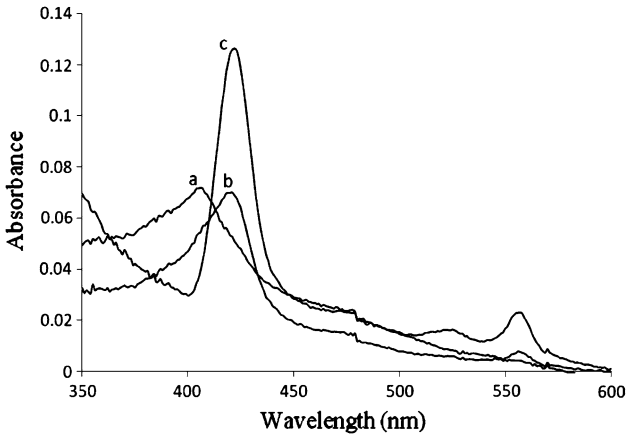

Fig. 1 Differential spectra of native POX_{1B} [0.67 μM in 25 mM tris(hydroxymethyl)aminomethane (Tris)–HCl pH 7.4]: *a* alone, *b* after addition of 0.2 mM pyridine, and *c* in the presence of 0.2 mM pyridine and 1 mM dithionite

with one molecule of pyridine bound to the iron on the distal face of the heme, or to a (protoporphyrin IX)Fe(II)(pyridine)$_2$ hemochromogen complex, bound to two molecules of pyridine, one of which had displaced the axial histidine ligand. These studies clearly show that the heme is the prosthetic group of the POX_{1B} protein.

The affinity of exogenous heme for the native form of POX_{1B} was analyzed by UV–vis spectroscopy (Fig. 2). For this purpose, difference UV–vis spectra were recorded with increasing concentrations of exogenous heme (hemin) from 0.03 to 1.2 μM in both reference and sample cuvettes containing the same concentration of native POX_{1B} in its oxidized and its reduced form, respectively. The differential spectra showed that the intensity of the Soret peak at 422 nm characteristic of reduced POX_{1B} in the sample cuvette increased and the peak at 406 nm characteristic of oxidized POX_{1B} in the reference cuvette decreased when the heme concentration was increased (Fig. 2). The shift of the Soret band of free heme in buffer solution from 396 nm (data not shown) to 406 nm, which is the same as that observed for the native form of POX_{1B}, indicates that the exogenous heme is correctly inserted within the active site of the apoprotein like in native POX_{1B}. Then, the POX_{1B} protein acquired heme from the hemin solution during the incubation in both the reduced and the oxidized form, which underlined the high affinity of POX_{1B} for hemin. These results are similar to those of reported interactions between different native apo-HRP (403 nm) and free synthetic heme (Soret band at 385 nm) [62]. To evaluate the affinity constant of the hemin for POX_{1B}, the variation of absorbance was plotted versus the concentration of the hemin added. The plot of $1/\Delta A_{422}$ versus the reciprocal of the hemin concentration is shown in the inset in Fig. 2. These curves allow one to evaluate the dissociation constant (K_d) of the heme–protein complex. K_d values were calculated considering the linear region and using the standard equation: $1/\Delta A = 1/\Delta A_\infty + K_d/[L]^n \times 1/\Delta A_\infty$, where $\Delta A = A - A_0$ and $\Delta A_\infty = A - A_\infty$, where A_0, A_∞, and A correspond to the absorbances of the initial, final, and mixed species in presence of a ligand, respectively, and [L] is the concentration of the ligand [63]. Two linear curves were obtained: the first one was obtained at low heme concentrations (under 0.15 μM), corresponding to the strong interaction of heme with the POX_{1B} in the active site with a dissociation constant (K_d) of approximately 1 nM; the second linear curve was obtained at higher heme concentration (0.15–1 μM), with a K_d of approximately 0.5 nM, and most probably corresponded to the nonspecific interaction and the adsorption of heme with the apoprotein. A study of the evolution of the absorption spectrum of POX_{1B} as a function of time was realized after each addition of an aliquot of hemin solution. No increase in the Soret peak's intensity was noted after 2 min (data not shown), which showed that the binding of the heme to the protein had reached the equilibrium. In further studies, it was then found that the reaction time necessary for the incorporation of exogenous heme into apo-POX_{1B} was less 2 min. Thus, the easy heme insertion into the pocket could

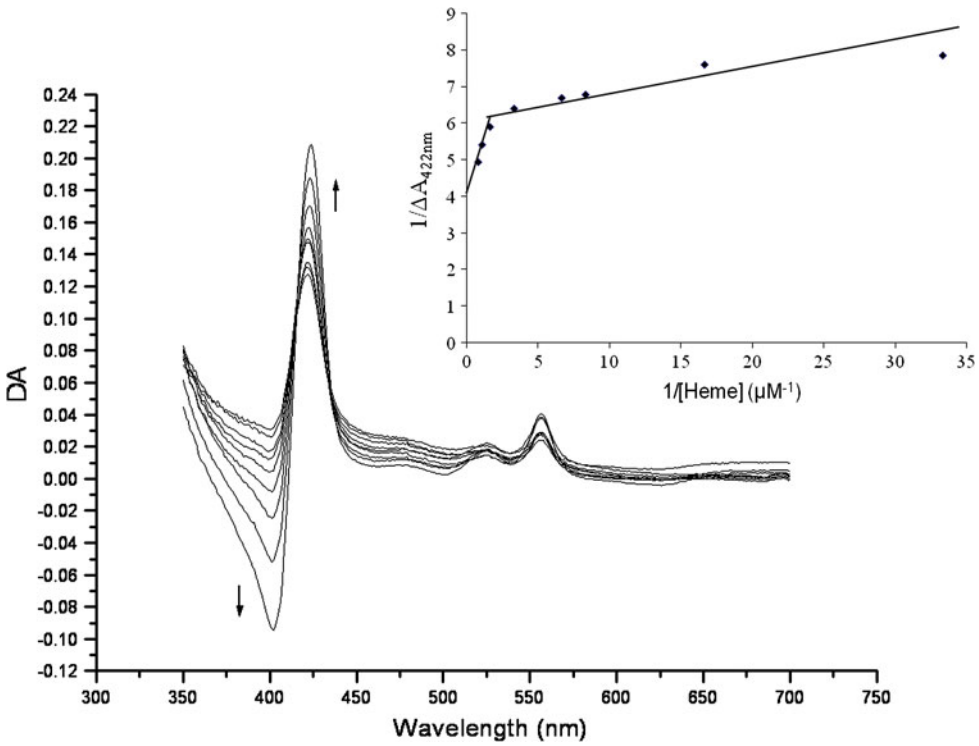

Fig. 2 Differential spectra of native POX_{1B} (0.67 μM in 25 mM Tris–HCl pH 7.4) in the presence of increasing heme concentrations (0.03–1.2 μM), 0.2 mM pyridine, and 1 mM sodium dithionite. The *inset* shows the curve of $1/\Delta A_{422}$ as a function of the reciprocal of the heme concentration

be attributed to high-affinity POX_{1B}–heme interactions. The structural properties of the protein could also be studied with regard to the heme neighboring and surrounding amino acid residues. The determination of the heme pocket peptides, especially the proximal ligand, is important to understand the structure–function relationships in this heme protein.

Determination of heme and the peptides in the heme pocket by MS

MS allows one to determine the mass of the heme using the MALDI–TOF technique. LC–MS/MS was performed to analyze the peptides in the protein and the peptides in the heme pocket. By MALDI–TOF under acetic conditions, the monoisotopic mass of the heme was measured at $m/z = 656.07$ (Fig. 3a). This corresponds to the theoretical mass of the heme with calcium—$(M+Ca)^+ = 656.14$—and confirms that iron(III) protoporphyrin IX is the prosthetic group of POX_{1B}.

The LC–MS/MS analysis of the protein allowed the identification of six peptides, and three of the matching residue sequences correspond to proteins with protoporphyrin IX containing iron ($C_{34}H_{32}FeN_4O_4$) (Table 1). In class III plant peroxidases, the active site and its surroundings, including the distal and proximal ligands, cysteine residues, and calcium binding sites, are among the conserved sequences. Therefore, the POX_{1B} protein can include similar structural features since homologies with HRP C1a were found. This protein contains two calcium ions, eight N-linked glycans, four disulfide bonds, and one heme group with conserved residues on the proximal side including Val164, His170, and Asp247 [64]. Collision-induced dissociation of peptide 2 precursor ions produced N-terminal b-type and C-terminal y-type ions according to the nomenclature of Roepstorff and Fohlmann [65] (Fig. 3b). Some of these ions (b_1, b_2, y_1, y_2) were not observed owing to the apparatus low mass cutoff. These informative b-type and y-type sequence ions were recorded in addition to nonsequence ions generated by the loss of

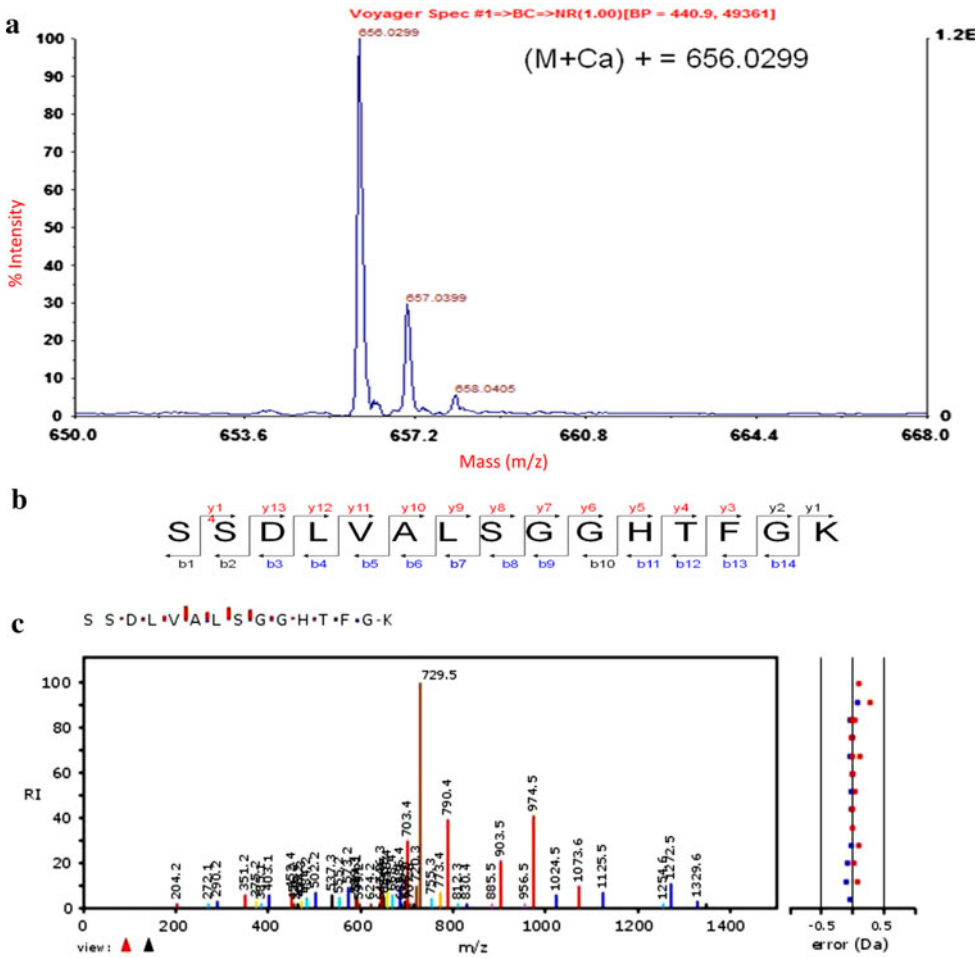

Fig. 3 **a** Matrix-assisted laser desorption/ionization time-of-flight mass spectrometry of heme. Monoisotopic mass of $(M+Ca)^+ = 656.07$ in positive ion mode. **b** Collision-induced-dissociation-based fragmentation of peptide 2; *blue* N-terminal b-type ions, *red* C-terminal y-type ions, **c** Electrospray ionization tandem mass spectrometry spectra of peptide 2 (SSDLVALSGGHTFGK) $m/z = 738.37$, with 2+ charge status $[(M+H)^+ = 1{,}475.7493]$ and an observed molecular mass of 0.0024 Da. Majority sequence ions, *blue* b-type ions, *red* y-type ions; nonsequence ions generated by the loss of small neutrals, *purple* and *turquoise* water, *orange* and *green* ammonium hydroxide. Scan 1,100/retention time, 19.5

Table 1 Localization of peptides identified by mass spectrometry on POX_{1B}

Sample	No.	Theoretical mass	Experimental mass	Delta mass (ppm)	Amino acid sequence	Cross-correlation score	Location in HRP C1a (P00433, UniProtKB)	Location in HRP C1a (P00433, Protein Data Bank)
Native	Peptide 1	1,380.6508	1,380.6483	1.08	R/TEKDAFGNANSAR/G	3.8	93–105	92–106
POX_{1B}	Peptide 2	1,475.7493	1,475.7468	1.6	R/SSDLVALSGGHTFGK/N	4.82	190–204	159–175
	Peptide 3	1,586.8323	1,586.8268	2.3	R/MGNITPLTGTQGQIR/L	3.87	314–328	313–329

Only peptides present in the heme pocket are shown. We used the sequence of horseradish peroxidase (*HRP*) (Swiss-Prot accession number P00433) for the number of peptides

water and ammonium hydroxide. The parent ion, 729.5, has a 2+ charge status by the loss of neutral NH_3 (Fig. 3c). The alignment of the amino acid fragment of this protein (peptide 2 in Table 1) shows the presence of residues corresponding to a typical proximal histidine region in *Arabidopsis* peroxidases (S/DLVALSGGHTFG/K). In HRP C, it is known that the fifth axial ligand of the heme iron is His170 located in tryptic peptide T8 (residues 160–174). Almost identical residues close to His170 were also found in turnip peroxidase [66]. Thus, by analogy with these peroxidases among others, LC–MS/MS results suggest that the heme iron (Fe^{3+}) of protein POX_{1B} is bound to the imidazole group of the histidine included in peptide 2 at position 12 (Table 1), which then acts as its fifth axial proximal ligand. Besides, it is known that in peroxidases, the proximal histidine possesses an imidazolate character that results from the binding of the carboxylate group of an aspartate residue to the nitrogen atom of the imidazole fifth ligand through a hydrogen bond, whereas the distal arginine and histidine play an important role in stabilizing bound anionic ligands [67]. The nature of the proximal ligand could help in understanding the heme–ligand interactions which are detailed in the following sections.

Axial coordination of exogenous ligands on the iron atom

The coordination of exogenous ligands was analyzed with two kinds of N-donor ligands, imidazole and pyridine. A decrease in absorbance and a 16-nm redshift of the Soret band is observed when increasing concentrations of pyridine are added to 0.6 μM oxidized POX_{1B} in 10 mM buffer pH 7.4 (Fig. 4). An isosbestic point appears at 413 nm, which suggests the presence of two chemical species depending on the heme coordination environment and the binding of one or two molecules of pyridine. The final spectrum with maxima at 419, 526, and 556 nm is characteristic of a low-spin hexacoordinate iron(III) species with two N-donor axial ligands [68]. The curve representing $1/\Delta A_{419}$ as a function of the reciprocal of the pyridine concentration (inset in Fig. 4) shows a nonlinear variation for pyridine concentrations higher than 2 mM. In contrast, this variation is linear when pyridine concentrations are lower than 2 mM. The calculated dissociation constant (K_d) considering the linear variation and using the standard equation cited above is approximately 0.90 ± 0.05 mM. By contrast, the curve representing $1/\Delta A_{419}$ as a function of the reciprocal of the square of the pyridine concentration shows a first, linear variation for pyridine concentrations higher than 2 mM. In this case, the calculated K_d considering the linear variation is approximately 2.20 ± 0.04 mM^2 ($C_{50} = 1.48$ mM). A second, nonlinear variation was noticed for pyridine concentrations below 2 mM. The presence of two types of variations suggests that depending upon its concentration, there are two phases for the coordination of pyridine on the iron of POX_{1B}. In the first phase, for pyridine concentrations lower than 2 mM, the iron ion is able to bind one molecule of pyridine *trans* to its fifth proximal histidine ligand with a K_d of about 0.90 ± 0.05 mM. In the second phase, after the free binding site has been occupied by a first molecule of pyridine in the presence of a slight excess of the exogenous ligand, further addition of excess pyridine as a strong iron ligand causes the cleavage of the iron–proximal histidine ligand bond, and the subsequent replacement of the proximal histidine ligand by a second molecule of pyridine with a K_d of about 2.20 ± 0.04 mM^2. The same analysis was realized with imidazole as an exogenous ligand. Figure 5 shows a decrease in the Soret absorption with a redshift of 10 nm when the imidazole concentration increased. The final spectrum with maxima at 419 and 503 nm is, like with pyridine, characteristic of a low-spin hexacoordinate iron(III) species with two N-donor axial ligands [68]. The inset in Fig. 5 shows two linear curves when $1/\Delta A_{419}$ is plotted as a function of the reciprocal of the imidazole concentration, which suggests that the iron of the POX_{1B} protein is able to bind two imidazole ligands. In fact, the binding of the first imidazole molecule occurs at low exogenous ligand concentrations (0.5–2 mM) with a K_d of approximately 0.03 ± 0.002 mM. The replacement of the histidine ligand by the second imidazole molecule occurs with a K_d of approximately 1.55 ± 0.05 mM in the presence of a large excess of exogenous ligand (2–4 mM). The results confirm that in the case of protein POX_{1B},

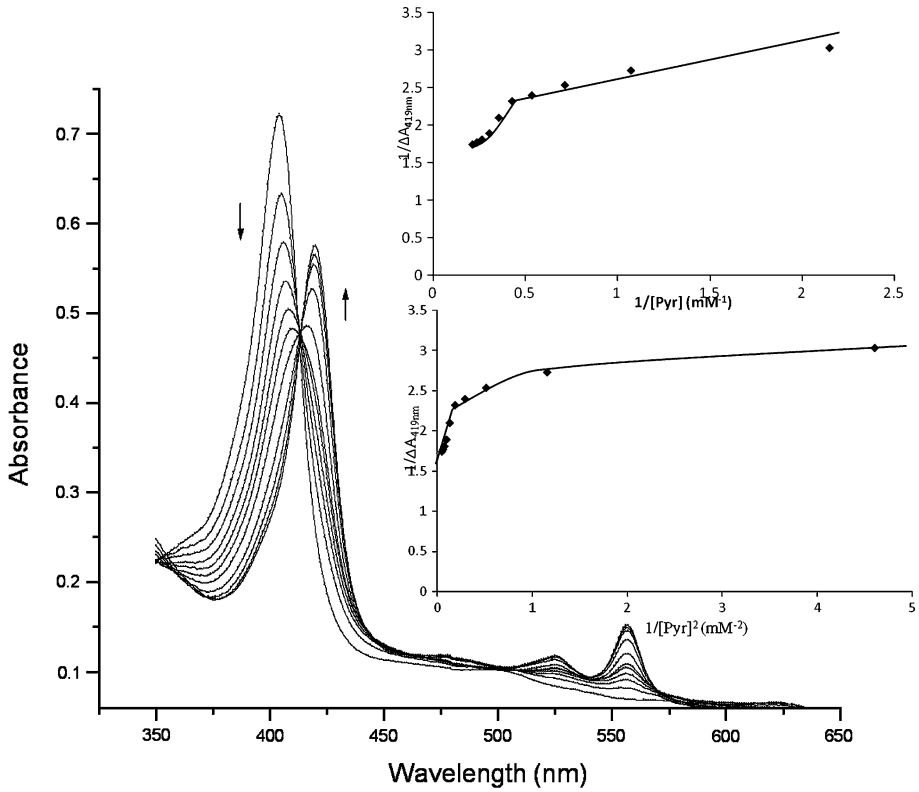

Fig. 4 Absolute spectra of reconstituted POX_{1B} [0.6 μM in 10 mM phosphate-buffered saline (PBS) pH 7.4] in the presence of increasing pyridine concentrations (0.45–3.37 mM). The *top inset* shows the curve of $1/\Delta A_{419}$ as a function of the reciprocal of pyridine concentration and the *bottom inset* shows the curve of $1/\Delta A_{419}$ as a function of the reciprocal of the square of pyridine concentration

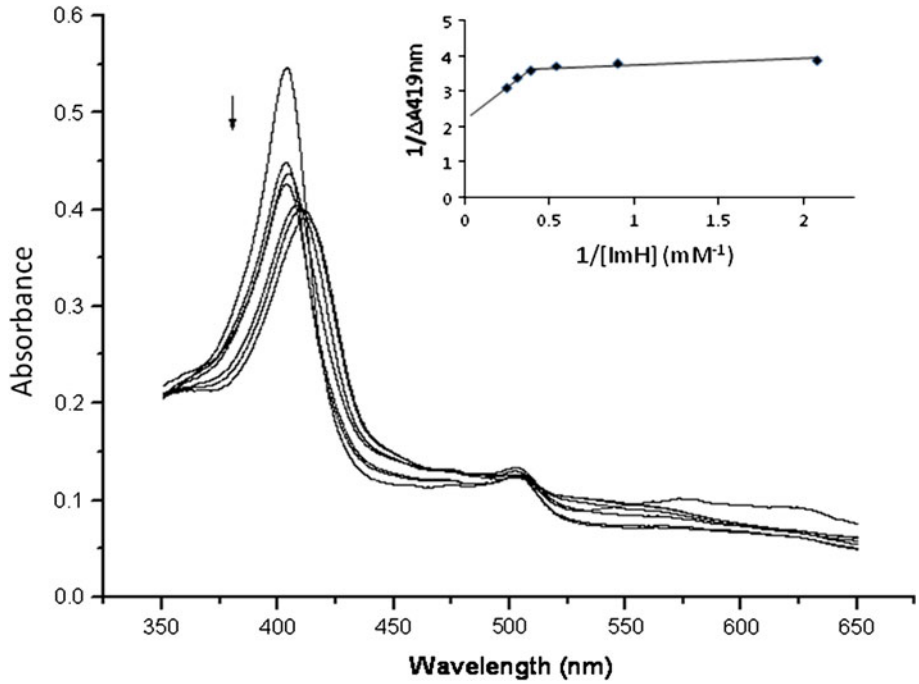

Fig. 5 Absolute spectra of reconstituted POX_{1B} (0.6 μM in 10 mM PBS pH 7.4) in the presence of increasing imidazole concentrations (0.48–4 mM). The *inset* shows curve of $1/\Delta A_{419}$ as a function of the reciprocal of imidazole concentration

imidazole can act as a sixth axial ligand of the iron atom. This was already demonstrated for microperoxidase 8 [69]. In the case of POX_{1B}, the binding of a second imidazole molecule, similarly to pyridine, by replacement of histidine is in concordance with the easy sixth ligand displacement by these two small molecules (i.e., imidazole and pyridine) observed in de novo heme proteins [70].

In heme proteins, the cleavage of the iron–proximal ligand bond is determined by the heme coordination geometry and the properties of the exogenous ligand. In

HRP and cytochrome *c* peroxidase [71, 72], the heme iron, in its stable form, is pentacoordinated and has a histidine as the proximal ligand: it is able to coordinate exogenous ligands such as CO. The complexation of the heme iron by exogenous ligands was also reported when the proximal histidine was mutated into a noncoordinating ligand: the formation of a pentacoordinate heme–hydroxide complex was reported in the case of mutated cytochrome *c* peroxidase and myoglobin [73, 74].

As a conclusion, in the POX_{1B} heme pocket, the proximal histidine ligand of the iron could be replaced in the presence of high exogenous ligand concentrations as already observed for HRP, cytochrome *c* peroxidase, and chloroperoxidase [71, 75].

The dissociation constants for pyridine ($K_d = 0.90 \pm 0.05$ mM) and imidazole ($K_d = 0.030 \pm 0.002$ mM) demonstrate the high affinity of the heme iron in POX_{1B} for these two exogenous ligands, for example, by comparison with chloroperoxidase that was reported to coordinate pyridine and imidazole with dissociation constants of 14 and 23 mM, respectively [74]. This peroxidase is, however, known to have heme coordination properties more similar to those of cytochrome P-450 than other peroxidases. In particular, the proximal ligand of its heme iron is a cysteine residue instead of a histidine residue present in most of the peroxidases. Higher dissociation constants have also been reported for iron–imidazole complexes of mutated cytochrome *c* peroxidase (2.7 mM) [76] and iron porphyrin–antibody complexes that possess a peroxidase activity (21.3 mM) [67]. In addition, an HRP H42A mutant, in which the distal histidine (His42) was mutated to alanine, was shown to be able to coordinate imidazole and 1-methylimidazole on its heme iron, but the formation of an imidazole–iron complex was observed only at a high imidazole concentration of 18 mM. With the same peroxidase, the dissociation constants were determined for unprotonated 1,2-dimethylimidazole and 2-methylimidazole and K_d values of 2.9 ± 1.3 and 2.5 ± 0.2 M, respectively, were measured, which confirmed the lower affinity of the heme iron for these nitrogen ligands [77]. The particularity of POX_{1B} in binding the exogenous ligand as well as the properties of the proximal ligand are of practical importance in controlling the catalytic performance, protein engineering, and functionalization [78, 79]. For example, an enhancement of the guaiacol and ABTS peroxidation by a recombinant HRP was noticed after the binding of an exogenous imidazole to the iron [77]. In fact, the specificity of binding imidazole compounds and pyridine derivatives by heme proteins is used to determine the affinity of the heme protein for exogenous N-donor ligands and allows one to evaluate the ability of the enzyme to bind ligands at the vacant sixth coordination site of the heme group.

It is well known that all plant peroxidases are characterized by the highly conserved peptides coordinating the heme moiety, but exhibit variability in the sequences controlling the accessibility of the active center, the so-called entrance to the heme binding pocket. Evaluation of binding properties of exogenous ligands gives information about the accessibility of the active site and its electronic properties and can help to predict, in the absence of an X-ray structure, the nature of some amino acid residues present in the heme pocket. Accordingly, the comparison of the coordination chemistry of peroxidases such as chloroperoxidase and mutated HRP H42A, which possess an amino acid other than histidine as the distal ligand of the iron, with that of garlic peroxidase suggests that histidine is probably the distal ligand in garlic peroxidase (POX_{1B}). In the case of POX_{1B}, both imidazole and pyridine are able to coordinate the heme and at high concentration can replace the axial ligand of the protein. POX_{1B} exhibited high affinity for both exogenous ligands, i.e., pyridine and imidazole, with a smaller dissociation constant for imidazole and, thus, a stronger binding ability. In the case of heme protein in a ferric state, the stability of the N-donor heme complex increases with the basicity of the ligand and its ability to donate electron density to the metal. In fact, it was demonstrated that such a ligand plays an important role in facilitating the dioxygen bond cleavage at the sixth coordination sites and stabilizing the hypervalent iron intermediates and then in enhancing the catalytic performance of peroxidases [18]. Regarding the properties of these two ligands, imidazole has higher basicity than pyridine as it is a σ-donor. In the case of pyridine, besides the σ-donor properties of nitrogen, it is a π-acceptor by its aromatic ring and so exhibits less coordination affinity for the heme of the POX_{1B} protein. Furthermore, in peroxidases, the proximal histidine ligand forms a hydrogen bond with an aspartate residue in the heme pocket. This His–Asp hydrogen bond plays a role in the tethering of the histidine ligand and its imidazolate character [31, 79]. As a consequence, the replacement of the proximal histidine by exogenous ligands could be related to the presence of an aspartate in the heme pocket forming a His–Asp bond in the case of garlic peroxidase POX_{1B}.

Electrochemical studies

Electrochemical measurements were undertaken to monitor the redox potential of the native and reconstituted POX_{1B} protein in solution and to characterize the effect of exogenous ligands on the redox potential. The redox potential of the reconstituted POX_{1B} protein [+0.46 V vs. the normal hydrogen electrode (NHE), pH 7.4] is close to that of the freshly purified native enzyme (+0.54 V vs. NHE, pH 7.4)

[51]. The slight difference in redox potential does not exclude the contribution of the interaction between the heme and the apoprotein due to the reconstitution process. The redox potential of the free heme in solution is reported to be +0.22 V versus the standard hydrogen electrode [69]. The redox potential of the heme center is controlled by the heme–protein interactions, the axial ligand coordination geometry, and the specific microenvironment of the protein [80, 81]. POX_{1B} exhibits a higher Fe(II)/Fe(III) redox potential than other heme peroxidases such as HRP (−0.278 V vs. NHE, pH 7.5), bovine lactoperoxidase (−0.310 V vs. NHE, pH 7.5), soybean peroxidase (SBP) (−0.191 V vs. NHE, pH 7.5), peroxidase from *Coprinus cinereus* UAMH 10067 (−0.183 V vs. NHE, pH 7.5), and versatile peroxidase from *Bjerkandera adusta* UAMH 8258 (+0.05 V vs. NHE, pH 7.5) [25]. The higher redox potential of the Fe(III)/Fe(II) couple would signify a higher electron deficiency within the active site. Ayala et al. [25] reported that the redox potential of the Fe(II)/Fe(III) couple in heme peroxidases could be related to their catalytic activity and demonstrated that the high redox potential of this redox couple is a signature of high oxidative capacity of the enzymatic reaction. Thus, the higher redox couple of POX_{1B} compared with other peroxidases is a signature of high catalytic activity. As a consequence, this peroxidase is able to oxidize substrates of higher oxidation–reduction potential. This finding is consistent with our previous results which reported high activity of the POX_{1B} protein in the presence of various peroxidase substrates such as chlorophenol derivatives [50].

The binding of an exogenous N-donor ligand to heme of POX_{1B} was monitored by measuring the shift of the potential after addition of various concentrations of pyridine (0.5, 1, and 1.7 mM). The redox potential of the Fe(III)/Fe(II) couple can be measured by cyclic voltammetry before and after addition of increasing pyridine concentrations. The iron–ligand complex was analyzed by measuring the redox potential at a sweep potential of −0.3 to +0.6 V. Figure 6 shows that the peak potential of the Fe(II)/Fe(III) redox couple shifted to more positive potential after pyridine binding, whereas the intensity of anodic and cathodic peaks decreased when pyridine was in excess (1 and 1.7 mM). Both the ferrous heme and the ferric heme showed shifts to more positive potentials. The shift in potential is due to the binding of ligand in both the oxidized and the reduced states of heme protein. The observed decrease in current may indicate that a high concentration of exogenous ligand leads to an exchange between pyridine and histidine and thus to the binding of the second pyridine molecule to the heme iron. The redox potential of the heme protein with the exogenous ligand shifted by 60 mV. It has already been reported that the binding of exogenous compounds such as N-donor ligands might shift the potential of the heme protein. In the case of pyridine, shifts of 0.071 and 0.149 V (reported values in the presence of 0.01 M pyridine) to a more positive potential were noticed for de novo heme protein S834C and isolated heme, respectively. The difference in shifts could be related to the partial blocking of accessibility to the heme by the protein scaffold [82]. The electrochemical studies as well as the recorded UV–vis spectra as detailed in the previous section suggest a high affinity of POX_{1B} for exogenous ligands, with a possible replacement of the proximal histidine. In addition to the structural features, the high redox potential could also be a determining factor in the catalytic activity of POX_{1B}.

Catalytic activity of POX_{1B}

The peroxidase activity was assayed in the presence of *o*-dianisidine as a reducing cosubstrate as detailed in "Materials and methods." The reconstituted POX_{1B} protein activity increased linearly as a function of exogenous heme quantities (0.06–0.15 μM) added to 0.01 μM native apo-POX_{1B} (Fig. 7). The mean RZ value (A_{406}/A_{280}) was 2.3, which suggests full heme occupancy and thus the production of a highly purified reconstituted protein. This value was approximately sixfold greater than that for the native protein. Compared with the native form, the reconstituted POX_{1B} showed an increase of activity proportional to the heme concentration, which suggests a correlation between the peroxidase structure and activity. The heme prosthetic group as well as amino acid residues are required for the catalytic activity of heme peroxidases since they play an important role in the cleavage of the peroxide bond. Several structural features, such as the coordination and the amino acid environment around heme, the hydrogen-

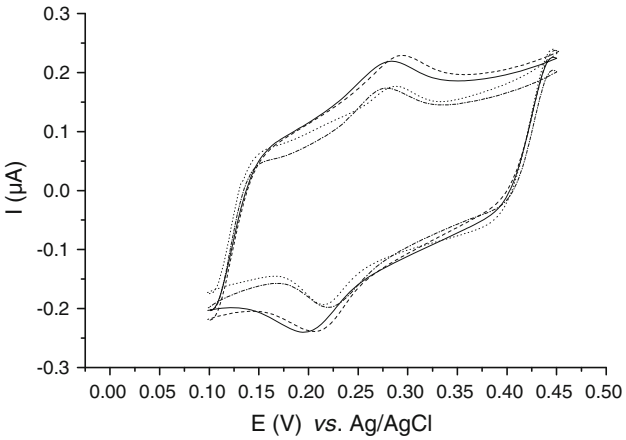

Fig. 6 Cyclic voltammograms recorded in the presence of reconstituted POX_{1B} (0.6 μM in 10 mM PBS pH 7.4) (*solid lines*) and after addition of increasing concentrations of pyridine: 0.5 mM (*dashed lines*), 1 mM (*dotted lines*), 1.7 mM (*dashed dotted lines*)

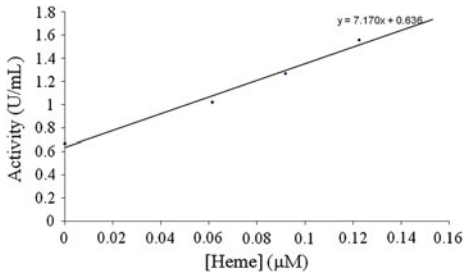

Fig. 7 Variation of the peroxidase activity of reconstituted POX_{1B}. Increasing heme concentrations (0.06–0.15 μM) were added to 0.01 μM apo-POX_{1B} in the reaction mix containing 100 mM sodium acetate pH 5.0 and the peroxidase activity was measured using the oxidation of 0.79 mM *o*-dianisidine by 10 mM H_2O_2 as described in "Materials and methods"

bonding network, the electrostatic charge distribution in the heme cavity, and the accessibility of heme to hydrogen peroxide and reducing substrates, contribute to the catalytic activity and efficiency of peroxidases. The correlation between the heme iron reactivity and the regulation of the electronic properties due to interactions between the proximal histidine and neighboring groups is also highlighted [83]. In the case of POX_{1B}, as a new peroxidase having not yet defined properties, the analysis of the affinity for some typical peroxidase substrates can help us to understand its catalytic activity.

Affinity for typical peroxidase substrates

The catalytic activity of reconstituted POX_{1B} protein was assayed in presence of typical peroxidase substrates (ABTS, TMB, *o*-dianisidine, guaiacol, H_2O_2). The determination of the rate-determining step of the catalytic cycle is necessary for the evaluation of the kinetic parameters of the reaction of POX_{1B} with such substrates. Under physiological conditions, compound I formation for plant peroxidases is generally very fast as shown by rate constants of 1.7×10^7 and 2×10^7 M^{-1} s^{-1}, respectively, for HRP C [84] and SBP [85]. Many literature reports show that HRP and its mutants, in which axial ligands are conserved, have a high rate constant for the formation of compound I. Some mutations of the residues located in the distal side of the heme pocket were performed and have demonstrated a small effect on the kinetics of the formation of compound I. For example, Smith and Veith [86] have demonstrated that the mutation of Arg38, which is involved in the cleavage of the peroxide O–O bond in the mechanism of formation of compound I, into various amino acids did not have any effect on the rate constant for the formation of compound I. Tanaka et al. [87] demonstrated that the mutation of Asp70 to valine or aspartate led to a decrease in the rate of compound I formation by less than 10%. The only mutation that caused a decrease in the rate of formation of compound I was that of the distal histidine, His42. The mutation of this amino acid into glutamate, which possesses general base properties similar to those of histidine, H42E, to obtain an active site mimic of chloroperoxidase, caused only a slight change in the rate constant of the formation of compound I. In contrast, if the distal histidine is mutated into glutamine or alanine a 10^6-fold lower rate constant is obtained. It is thus clear that the distal His42 is crucial for the formation of compound I, whereas Arg38 can be mutated with no change in the rate constant for the formation of compound I.

In the case of garlic peroxidase (POX_{1B}), it was proven by LC–MS/MS that the proximal ligand is His170. However, the residues in the distal heme pockets have not yet been clearly identified, although the presence of histidine and aspartate on the distal side of the heme pocket was suggested by LC–MS/MS studies.

A first experiment was performed to evaluate the rate of the reaction of POX_{1B} with hydrogen peroxide. The decrease in absorbance of the Soret band was measured as a function of time at various concentrations of hydrogen peroxide ranging between 1 and 11 mM, which allowed us to calculate a rate constant for this reaction of 30 s^{-1}. This rate takes into account both the formation of compound I and the subsequent oxidative destruction of the heme of POX_{1B} in the absence of any reducing cosubstrate. This rate is much higher than the pseudo-first-order rate constants that were determined in the presence of increasing concentrations of reducing substrates (1–4 s^{-1}, Table 2). We can then assume by analogy that the formation of compound I in the case of POX_{1B} is rapid and follows the same mechanism as for plant class III peroxidase, for which the rate-limiting step is usually that of the reaction of the enzyme intermediate compound II with the reducing substrate [88].

k_{cat} and apparent K_M values were then determined from Lineweaver–Burk plots considering concentrations from 0.01 to 0.1 mM for ABTS and TMB, and from 0.1 to 1 mM for *o*-dianisidine and guaiacol (Fig. 8). The reported values are an average of six values. The K_M values for *o*-dianisidine and guaiacol in the presence of 10 mM optimized concentration of H_2O_2 were 71.9 ± 0.9 and 96 ± 1.0 μM, respectively. POX_{1B} had a higher affinity for ABTS and TMB since the apparent K_M values were 10 ± 1.0 and 4.7 ± 0.7 μM, respectively. In the presence of a saturating concentration of *o*-dianisidine as a reducing substrate, the apparent K_M value for H_2O_2 was 0.11 mM. The affinity constant for ABTS is higher than that obtained for SBP (173 ± 9 μM) and for HRP C (178 ± 8 μM) [83] POX_{1B} also showed higher affinity for *o*-dianisidine compared with microperoxidase 8, having an apparent K_M of 0.4 mM [61]. The affinity of peroxidase for different substrates can

Table 2 Kinetic parameters for the oxidation of various reducing cosubstrates by H_2O_2 catalyzed by 1 μM reconstituted POX_{1B} in 0.1 M sodium acetate buffer pH 5.0

Substrate	K_M (μM)	V_{max} (U min^{-1})	k_{cat} (turnovers s^{-1})	k_{cat}/K_M (mM^{-1} s^{-1})
ABTS	10 ± 1.0	27.0 ± 0.6	3.82 ± 0.08	400 ± 30
TMB	4.7 ± 0.7	13.7 ± 0.5	1.93 ± 0.05	411 ± 44
o-Dianisidine	71.9 ± 0.9	5.9 ± 0.2	1.18 ± 0.15	17 ± 1.5
Guaiacol	96 ± 1.0	4.9 ± 0.1	1.00 ± 0.20	11 ± 2
H_2O_2[a]	116.1 ± 0.9	10.7 ± 0.5	1.20 ± 0.04	10 ± 0.3

ABTS 2′-azinobis(3-ethylbenzothiazoline-6-sulfonic acid), *TMB* 3,3′,5,5′-tetramethylbenzidine

[a] Kinetic parameters determined in the presence of a saturating concentration of *o*-dianisidine (0.79 mM)

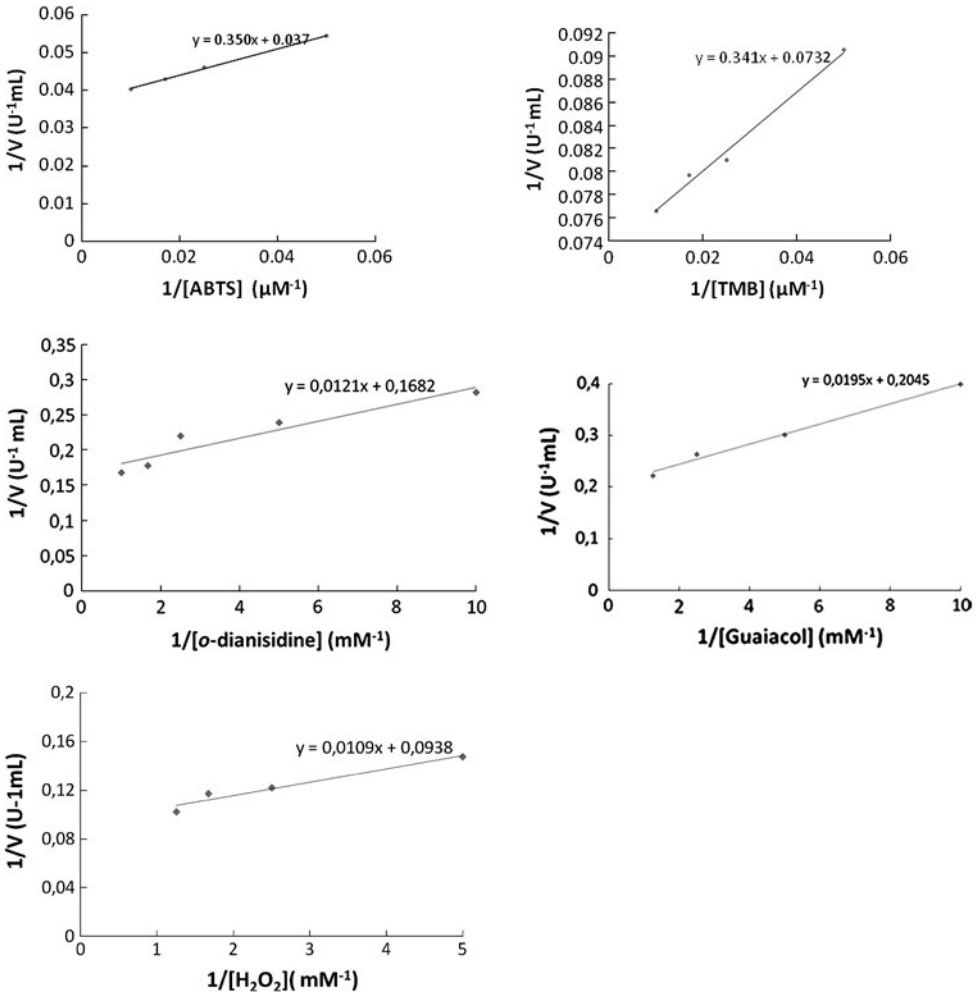

Fig. 8 Lineweaver–Burk plots. Concentrations varied between 0.01 and 0.1 mM for 2,2′-azinobis (3-ethylbenzothiazoline-6-sulfonic acid) (*ABTS*) and 3,3′,5,5′-tetramethylbenzidine (*TMB*), and between 0.1 and 1 mM for *o*-dianisidine and guaiacol. The reactions were performed in the presence of 10 mM H_2O_2 as an oxidant. All measurements were made at optimal pH and ionic strength (0.1 M sodium acetate buffer pH 5) and at 25 °C using 2 μM POX_{1B} in 10 mM PBS pH 7.4

help to predict reaction mechanisms and the properties of the active center in terms of accessibility and electronic properties. In the case of POX_{1B}, the order of affinity of the enzyme for different substrates was TMB > ABTS > *o*-dianisidine > guaiacol. Such an order defines a different mechanism for substrate binding sites compared with the other peroxidases. For example, in the case of guaiacol peroxidase isolated from corn root plasma membranes, the first isoform (pmPOX1) showed the following affinity order *o*-dianisidine > guaiacol > TMB » ABTS, whereas the second isoform (pmPOX2) showed higher affinity for TMB than for guaiacol [89]. In the case of anionic plant peroxidases such as tobacco peroxidase, the negatively charged pocket owing to the presence of glutamate instead of phenylalanine influences enzyme reactivity toward donor substrates [58]. The difference in reactivity with these substrates in comparison with other peroxidases suggests that garlic peroxidase (POX_{1B}) possesses different

structural properties which can be elucidated by a further crystal characterization.

The catalytic activity (k_{cat}) and catalytic efficiencies (k_{cat}/K_M) were calculated using turnover numbers (k_{cat}) determined by dividing V_{max} by the protein concentration and the affinity constant for the substrate. The reported values of catalytic activity toward ABTS ($k_{cat} = 3.80\ s^{-1}$) in Table 2 are, however, significantly lower than those for other heme peroxidases such as HRP C ($k_{cat} = 736\ s^{-1}$) or SBP ($k_{cat} = 1{,}230\ s^{-1}$) and HRP isoenzyme ($k_{cat} = 37\ s^{-1}$) [90]. In the case of POX_{1B}, the catalytic efficiency determined by k_{cat}/K_M ($400\ mM^{-1}\ s^{-1}$) for ABTS was higher than that reported for other peroxidases such as SBP ($7.1\ mM^{-1}\ s^{-1}$) and HRP C ($4.1\ mM^{-1}\ s^{-1}$) as a result of a low K_M value (9.5 μM). The same behavior is observed for TMB, for which a k_{cat}/K_M value of $411\ mM^{-1}\ s^{-1}$ was calculated. In the presence of guaiacol, the pseudo-first-order k_{cat} and K_M apparent values obtained with POX_{1B} (see Table 2) are 0.095 mM and $1.01 \pm 0.02\ s^{-1}$, respectively, which leads to a catalytic efficiency of $11 \pm 2\ mM^{-1}\ s^{-1}$. By comparison, in the case of HRP isoenzyme [88] the values reported are $k_{cat} = 1107 \pm 72\ s^{-1}$ and $K_M = 5.0$ mM, which lead to a catalytic efficiency of $221\ mM^{-1}\ s^{-1}$. These results demonstrate once again that the catalytic activity characterized by the turnover is lower than that reported for other plant peroxidases, the high catalytic efficiency observed being due to a high binding affinity for the substrate. Guaiacol, *o*-dianisidine, ABTS, and TMB are aromatic electron donors. The binding affinity depends on the nature of the aromatic residue at the side chain of the protein, the electron donating efficiency of the substrate, and the electrostatic charge distribution in the heme cavity. The catalytic efficiency is largely influenced by the accessibility of the heme to peroxidase substrates, which correlates with the structural properties of the enzyme. POX_{1B} exhibited good affinity for typical peroxidase substrates and lower catalytic turnover rates than other peroxidases. This suggests that this garlic peroxidase might provide high efficiency as a catalyst in various reaction mechanisms which could result, for some reactants, in stable complexes with the heme protein.

Formation of iron(II) nitrosoalkane complexes

The covalent binding of the –SH groups of proteins might occur in presence of nitrosoalkanes, which are instable intermediates reacting generally with glutathione or cysteine. This property is important in the oxidative metabolism of drugs such as macrolides. The ability of the enzyme to demethylate and oxidize such molecules into nitrosoalkanes leads to the generation of stable and inactive complexes suitable for remediation of adverse effects of some drug derivatives [91]. The experiments detailed below deal with this ability to form nitrosoalkane complexes, which was only demonstrated for some peroxidases. In the case of the new garlic peroxidase (POX_{1B}), the reduction of 1-nitrohexane was assayed under strictly anaerobic conditions, in the presence of 1 mM sodium dithionite as a reducing agent and POX_{1B} (0.6 μM in 10 mM PBS pH 7.4). Under those conditions, a shift of the Soret band to 411 nm was first observed, corresponding to the heme iron reduction leading to iron(II)–POX_{1B}. Further addition of increasing concentrations of 1-nitrohexane (0.1–0.8 mM) led to an additional redshift of 3 nm, concomitant with a decrease in absorbance (Fig. 9). This result was consistent with the results obtained in the case of the formation of iron(II) nitrosoalkane complexes of microperoxidase 8 [39] and other heme proteins [41]. Therefore, it is likely that the formation of a similar iron nitrosoalkane complex occurred by formation of a strong bond between the nitrosoalkane ($C_6H_{13}NO$) and the POX_{1B}–Fe(II) produced, respectively, after the reduction of the nitroalkane compound ($C_6H_{13}NO_2$) and the POX_{1B}–Fe(III) in the presence of sodium dithionite. Thus, the coordination chemistry of the POX_{1B} protein offers new applications in the pharmaceutical field. For example, protein–iron(II) nitrosoalkane complexes upon in situ oxidation of drugs having primary or secondary amine functions such as N-substituted hydroxylamines have an inhibitory effect on monooxygenase activities [43]. These enzymes are involved in vivo in drug metabolism such as the oxidative metabolism of xenobiotics in humans [92].

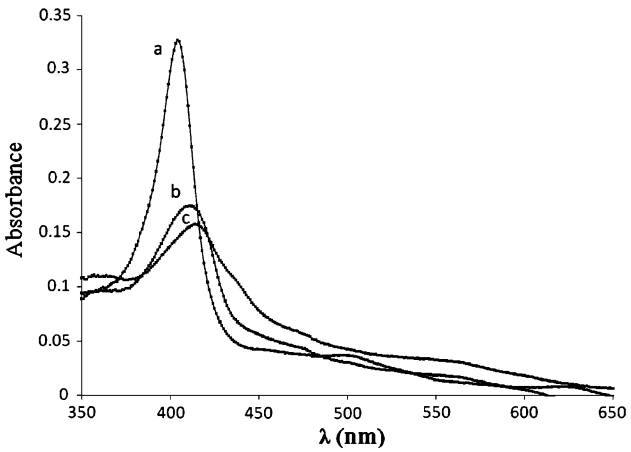

Fig. 9 Reaction of POX_{1B} (0.6 μM in 10 mM PBS pH 7.4) with 1-nitrohexane (0.1–0.8 mM): *a* spectrum of oxidized POX_{1B}, *b* spectrum obtained after addition of 1 mM sodium dithionite, and *c* spectrum of POX_{1B} in the presence of 1 mM sodium dithionite and 1-nitrohexane

Conclusion

In this paper, we have characterized structural coordination features of a new garlic peroxidase (POX_{1B}). The heme and the axial ligands are key components of the active site in heme proteins since they are involved in enzyme functions such as oxidation/reduction of a wide range of substrates, electron transfer, and coordination of exogenous substrates. Structural characterization by UV–vis spectroscopy and LC–MS/MS was performed. The results demonstrated the presence of a prosthetic group typical of iron(III) porphyrins with histidine as a proximal ligand of the iron center. Exogenous ligands such as pyridine and imidazole easily bind to the iron atom and can generate axial ligand switching. Furthermore, the POX_{1B} heme protein shows a high affinity for typical peroxidase substrates such as *o*-dianisidine, guaiacol, TMB, ABTS, and hydrogen peroxide. The catalytic efficiency of this peroxidase demonstrates a great potential to be exploited for different reaction mechanisms. This is of practical importance especially when it is applied for biosensor applications such as the sensing of hydrogen peroxide or a reducing substrate of biological or chemical interest as the increase in the catalytic activity can be expressed in terms of current response. In the presence of nitro compounds, a POX_{1B}–iron(II) nitrosoalkane complex is produced, which is another interesting point demonstrating the versatility of this enzyme thanks to its coordination chemistry. The ability to form nitrosoalkane complexes is particularly interesting in the case of drug metabolism, for example, in the case of xenobiotics or macrolide antibiotics, when nitroso intermediates are derived from amine functions, leading to reactive metabolites or intermediates. Finally, the study of the structure–activity relationship of this new garlic peroxidase reported in this work will help in the development of new biosensing devices for specific target molecules as catalytic substrates or coordinated ligands.

Acknowledgments This work was supported by a cooperation project between the CNRS (France) and DGRSRT (Tunisia). Financial support from the Tunisian Ministry of High Education, Scientific Research and Technology and Paris-Sud 11 University is gratefully acknowledged.

References

1. Wakamatsu K, Takahama U (1993) Physiol Plant 68:167–171
2. Biles CL, Martyn RD (1993) Plant Physiol Biochem 31:499–506
3. Lin ZF, Chen LH, Zhang WQ (1996) Process Biochem 5:443–448
4. Krell HW (1991) In: Loburzewski J, Greppin H, Penel C, Gaspar T (eds) Biochemical, molecular and physiological aspects of plant peroxidases. University of Maria Curie-Sklodowska, Lublin, and University of Geneva, Geneva, pp 469–478
5. Chiou CC, Chang PY, Chan EC, Wu TL, Tsao KC, Wu JT (2003) Clin Chem Acta 334:87–94
6. Agostini E, Hernandez-Ruiz J, Arnao MB, Milrand SR, Tigier HA, Acosta M (2002) Biotechnol Appl Biochem 35:1–7
7. Ruzgas T, Csoregi E, Katakis I, Kenausis G, Gorton L (1996) J Mol Recognit 9:480–484
8. Marzouki SM, Limam F, Smaali MI, Ulber R, Marzouki MN (2005) Appl Biochem Biotechnol 127:201–214
9. Chen S, Yuan R, Chai Y, Yin B, Li W, Min L (2009) Electrochem Acta 54(11):3039–3046
10. Fawer MS, Stierli J, Cliffe S, Fiechter A (1991) Biochim Biophys Acta 1076:15–22
11. Nicolis S, Casella L, Roncone R, Dallacosta C, Monzani E (2007) C R Chim 10:380–391
12. Poulos TL, Freer BT, Alden RA, Edwards SL, Skoglund U, Takio K, Eriksson B, Xuong N, Yonetani Y, Kraut J (1980) J Biol Chem 255:575–580
13. Poulos TL, Edwards SL, Wariishi H, Gold MH (1993) J Biol Chem 268:4429–4440
14. Patterson WR, Poulos TL, Goodin DB (1995) Biochemistry 34:4342–4345
15. Schuller DJ, Ban N, van Huystee RB, McPherson A, Poulos TL (1996) Structure 4:311–321
16. Gajhede M, Schuller DJ, Henriksen A, Smith AT, Poulos TL (1997) Nat Struct Biol 4:1032–1038
17. Welinder KG (1992) Curr Opin Struct Biol 2:388–393
18. Poulos TL (1996) J Biol Inorg Chem 1:356–359
19. Jensen KP, Ryde U (2003) Mol Phys 13:2003–2018
20. Veitch NC (1993) NMR studies of peroxidases. Thesis, Oxford University
21. Hatefi Y (1985) Annu Rev Biochem 54:1015–1069
22. Narula J, Pandey P, Arbustini E, Haider N, Narula N, Kolodgie FD, Dal Bello B, Semigran MJ, Bielsa-Masdeu A, Dec GW, Israels S, Ballester M, Virmani R, Saxena S, Kharbanda S (1999) Proc Natl Acad Sci USA 96:8144–8149
23. Yoshikawa S (2002) Adv Protein Chem 60:341–342
24. Dunford HB (1999) Heme peroxidases. Wiley-VCH, New York
25. Ayala M, Roman R, Vazquez-Duhalt R (2007) Biochem Biophys Res Commun 357:804–808
26. Chuang W-J, Chang Y-D, Jeng W-Y (1999) J Inorg Biochem 75:93–97
27. Adams PE (1991) In: Everse J, Everse KE, Grisham MB (eds) Peroxidases in chemistry and biology, vol 2. CRC Press, Boca Raton
28. Louro RO, Correia IJ, Brennan L, Coutinho IB, Xavier AV, Turner DL (1998) J Am Chem Soc 120:13240
29. Walker FA (2004) Chem Rev 104:589–615
30. Momenteau M (1986) Pure Appl Chem 58(11):1493–1502
31. Buffard D, Breda C, van Huystee RB, Asemota O, Pierre M, Dang HDB, Esnault R (1990) Proc Natl Acad Sci USA 87:8874–8878
32. Loew GH, Harris DL (2000) Chem Rev 100:407–419
33. de Visser SP (2006) J Biol Inorg Chem 11:168–178
34. Rath SP, Olmstead MM, Balch AL (2004) J Am Chem Soc 126:6379–6386
35. Erman JE, Vitello LB, Miller MA, Shaw A, Brown AK, Kraut J (1993) Biochemistry 32(37):9798–9806
36. Newmyer SL, de Montellano PRO (1995) J Biol Chem 270:19430–19438
37. Tanaka M, Nagano S, Ishimori K, Morishima I (1997) Biochemistry 36:9791–9798
38. Howes BD, Schiødt CB, Welinder KG, Marzocchi MP, Ma J-G, Zhang J, Shelnutt JA, Smulevich G (1999) Biophys J 77:478–492
39. Ricoux R, Boucher J-L, Mansuy D, Mahy J-P (2000) Biochem Biophys Res Commun 278:217–223
40. Porter DJT, Bright HJ (1983) J Biol Chem 258(16):9913–9924

41. Mansuy D, Beaune P, Cresteil T, Bacot C, Chottard JC, Gans P (1978) Eur J Biochem 86:573–579
42. Mansuy D, Chottard JC, Chottard G (1977) Eur J Biochem 76:617–623
43. Mahy JP, Mansuy D (1991) Biochemistry 30:4165–4172
44. Lee J, Chen L, West AH, Richter-Addo GB (2002) Chem Rev 102:1019–1065
45. Mansuy D, Battioni P, Chottard J-C, Riche C, Chiaroni A (1983) J Am Chem Soc 105:455–463
46. Bensoussan C, Delaforge M, Mansuy D (1995) Biochem Pharmacol 49(5):591–602
47. Kajita J, Inano K, Fuse E, Kuwabara T, Kobayashi H (2002) Drug Metab Dispos 30(12):1504–1511
48. El Ichi S, Abdelghani A, Hadji I, Helali S, Limam F, Marzouki MN (2008) Biotechnol Appl Biochem 51:33–41
49. El Ichi S, Limam F, Marzouki MN (2009) Mater Sci Eng C 29(5):1662–1667
50. El Ichi S, Marzouki MN, Korri-Youssoufi H (2009) Biosens Bioelectron 24(10):3084–3090
51. Bradford M (1976) Anal Biochem 72:248–254
52. Rudrappa T, Neelwarne B, Kumar V, Lakshmanan V, Venkataramareddy SR, Aswathanarayana RG (2005) Electron J Biotechnol 8(2):185–196
53. Laemmli UK (1970) Nature 227:680–685
54. Hoopes JT, Dean JFD (2001) Anal Biochem 293:96–101
55. Hiraga S, Sasaki K, Ito H, Ohashi Y, Matsui H (2001) Plant Cell Physiol 42:462–468
56. Paul K-G, Stigbrand T (1970) Acta Chem Scand 24:3607–3617
57. Pahari D, Patel AB, Behere DV (1995) J Inorg Biochem 60:245–255
58. Gazaryan IG, Lagrimini LM (1995) Phytochemistry 41(4):1029–1034
59. Wariishi H, Akileswaran L, Gold M (1988) Biochemistry 27:5365–5370
60. Gaspard S, Chottard G, Mahy J-P, Mansuy D (1996) Eur J Biochem 238:529–537
61. Ricoux R, Sauriat-Dorizon H, Girgenti E, Blanchard D, Mahy J-P (2002) J Immunol Methods 269:39–57
62. Song H-Y, Liu J-Z, Weng L-P, Ji L-N (2009) J Mol Catal B Enzym 57:48–54
63. Brault D, Rougee M (1974) Biochem Biophys Res Commun 3:654–659
64. Flocco CG, Alvarez MA, Giulietti AM (1998) Biotechnol Appl Biochem 28:33–38
65. Roepstorff P, Fohlmann J (1984) Biomed Mass Spectrom 11:601
66. Welinder KG, Mazza G (1977) Eur J Biochem 73:353–358
67. Heering HA, Jansen MAK, Thorneley RNF, Smulevich G (2001) Biochemistry 40:10360–10370
68. De Lauzon S, Mansuy D, Mahy J-P (2002) Eur J Biochem 269:470–480
69. Ricoux R, Korri-Youssoufi H, Mahy J-P (2005) J Biol Sci 5(1):44–49
70. Das A, Hecht MH (2007) J Inorg Biochem 101:1820–1826
71. Dasgupta S, Rousseau DL, Anni H, Yonetani T (1989) J Biol Chem 264:654–662
72. Uno T, Nishimura Y, Tsuboi M, Makino R, Iizuka T, Ishimurali Y (1987) J Biol Chem 262(10):4549–4556
73. Sun J, Fitzgerald MM, Goodin DB, Loehr TM (1997) J Am Chem Soc 119:2064–2065
74. Das TK, Franzen S, Pond A, Dawson JH, Rousseau DL (1999) Inorg Chem 38:1952–1953
75. Sono M, Dawson JH, Hall K, Hager LP (1986) Biochemistry 25:347–356
76. Mcree DE, Jensen GM, Fitzgerald MM, Siegel HA, Goodin DB (1994) Proc Natl Acad Sci USA 91:12847–12851
77. Newmeyer SL, de Montellano PRO (1996) J Biol Chem 271(25):14891–14896
78. Roncone R, Monzani E, Murtas M, Battaini G, Pennati A, Sanangelantoni AM, Zuccotti S, Bolognesi M, Casella L (2004) Biochem J 377:717–724
79. Newmyer SL, Sun J, Loehr TM, de Montellano PRO (1996) Biochemistry 35:12788–12795
80. Tezcan FA, Winkler JR, Gray HBJ (1998) Am Chem Soc 120:1338
81. Willner I, Heleg-Shabtai V, Katz E, Rau HK, Haehnel W (1999) J Am Chem Soc 121:6455–6468
82. Das A, Trammell SA, Hecht MH (2006) Biophys Chem 123:102–112
83. Poulos TL, Kraut J (1980) J Biol Chem 255:8199–8205
84. Smith AT, Sanders SA, Thorneley RNF, Burke JF, Bray RC (1992) Eur J Biochem 207:507–519
85. Kamal JKA, Behere DV (2003) J Inorg Chem 94:236–242
86. Smith AT, Veith NC (1998) Curr Opin Chem Biol 2:269–278
87. Tanaka M, Morimoto A, Ishimori K, Morishima I (1998) Pure Appl Chem 70(4):911–916
88. Rodriguez-Lopez JN, Smith AT, Thorneley RNF (1996) J Biol Inorg Chem 1:136–142
89. Mika A, Lüthje S (2003) Plant Physiol 132:1489–1498
90. Gil-Rodríguez P, Ferreira-Batista C, Vázquez-Duhalt R, Valderrama B (2008) Eng Life Sci 8(3):286–296
91. Pessayre D, Larrey D, Funck-Brentano C, Benhamou JP (1985) J Antimicrob Chemother 16:181–194
92. Benedetti MS, Tipton KF, Whomsley R (2007) Fundam Clin Pharmacol 21:467–480